

Competing Many-Body Phases at Small Fillings in Ultrahigh-Quality GaAs 2D Hole Systems: Role of Landau Level Mixing

Chengyu Wang,¹ A. Gupta,¹ S. K. Singh,¹ L. N. Pfeiffer,¹ K. W. Baldwin,¹ R. Winkler,² and M. Shayegan¹

¹*Department of Electrical and Computer Engineering,
Princeton University, Princeton, New Jersey 08544, USA*

²*Department of Physics, Northern Illinois University, DeKalb, Illinois 60115, USA*

(Dated: March 28, 2025)

The fractional quantum Hall state (FQHS), an incompressible liquid state hosting anyonic excitations with fractional charge and statistics, represents a compelling many-body phase observed in clean two-dimensional (2D) carrier systems. The expected non-Abelian nature of the FQHSs at even-denominator Landau level (LL) fillings has particularly sparked considerable recent interest. At sufficiently small fillings, another exotic phase, namely a quantum Wigner crystal (WC) state, dominates. Here we report magneto-transport measurements in an ultrahigh-quality GaAs 2D *hole* system where the large hole effective mass leads to a significant LL mixing (LLM) even at very high magnetic fields and affects the many-body states at very small fillings. We observe numerous developing FQHSs at both even- and odd-denominator fillings, deep in the insulating regime at $\nu \lesssim 1/3$ where WC states dominate. The FQHSs we observe at odd-denominator fillings on the flanks of $\nu = 1/4$ and $1/6$ are consistent with the Abelian Jain sequence of four-flux and six-flux composite fermions, while the ones at even-denominator fillings $\nu = 1/4$ and $1/6$ are likely non-Abelian states emerging from the pairing of these quasiparticles induced by severe LLM. Our results demonstrate that the competition between the FQHSs and WC phases is close at very small fillings even in the presence of severe LLM. We also measure activation energies of WC states near $\nu = 1/6$, and find that they are substantially larger than what has been reported for ultrahigh-quality GaAs 2D electrons. A moderate LLM is believed to lower the activation energy associated to the formation of WC intrinsic defects. The surprisingly large activation energy for our 2DHS with significant LLM is therefore puzzling, and may suggest a different type of intrinsic WC defect compared to that in 2D electrons.

I. INTRODUCTION

Low-disorder, two-dimensional (2D) charged carrier systems subjected to large perpendicular magnetic fields at low temperatures are consummate platforms for the study of many-body quantum phenomena thanks to the quenched thermal and kinetic energies. When the lowest-energy Landau level (LL) is partially occupied, the dominant electron-electron Coulomb interaction leads to the emergence of a variety of strongly-correlated, many-body quantum phases [1–4]. At sufficiently small LL fillings (ν), a disorder-free (ideal) 2D electron system (2DES) is expected to form an ordered array, the so-called quantum Wigner crystal (WC) [5], when the long-range part of Coulomb interaction is dominant. In realistic (non-ideal) samples, the many-body electronic crystal breaks into domains pinned by ubiquitous disorder, exhibiting a highly-insulating behavior [6]. Evidence for pinned WC phases has been reported in the lowest LL of different 2D systems, including GaAs 2D electrons [7–12] and holes [13–15], AlAs [16, 17], ZnO [18], and bilayer graphene [19]. At certain rational fractional fillings, the fractional quantum Hall state (FQHS), a strongly-correlated, incompressible liquid with nontrivial topological properties, manifests itself as the ground state thanks to the strong short-range electron-electron correlation [1–4]. The fractional charge and anyonic statistics [20–22], as well as the potentially non-Abelian nature of the quasiparticle excitations of even-denominator FQHSs [23–25] have further

sparked intense research interest in recent years.

A partially filled lowest LL with small fillings is of particular interest because it serves as the battleground for fundamental liquid and solid phases of interacting carriers. Experiments on ultrahigh-quality GaAs 2DESs revealed evidence for developing FQHSs at specific, extremely small fillings, e.g., at $\nu = 1/7$ [26–29], although insulating phases become dominant in filling ranges $1/5 < \nu < 2/9$ and $\nu < 1/5$ [8–12]. These observations signal the intricate competition between strongly correlated liquid and solid states, namely, FQHSs and a quantum WC.

In GaAs 2D *hole* systems (2DHSs), the larger effective mass ($\sim 0.5m_0$ [30]) compared to electrons ($0.067m_0$) suppresses the LL separation at high B , leading to a significant mixing of higher LLs into the many-body ground states of the lowest LL [32, 33]. Such mixing is quantified by the LL mixing (LLM) parameter κ , defined as the ratio of Coulomb energy E_{Coul} and cyclotron energy E_{cyc} . LLM explicitly breaks the particle-hole symmetry within a LL [31]. More importantly, it can modify the electron-electron interaction and play an important role in the stabilization of different correlated states in both lowest and excited LLs [13–17, 34–42]. For example, moderate LLM can affect the candidate non-Abelian FQHS at $\nu = 5/2$ [34, 35, 42]. In the lowest LL of dilute GaAs 2DHSs, severe LLM leads to the onset of insulating phases near $\nu \sim 1/3$ [13–15] rather than $\nu \sim 1/5$. This is because LLM softens the short-range part of Coulomb interaction, thereby favoring the formation of WC states

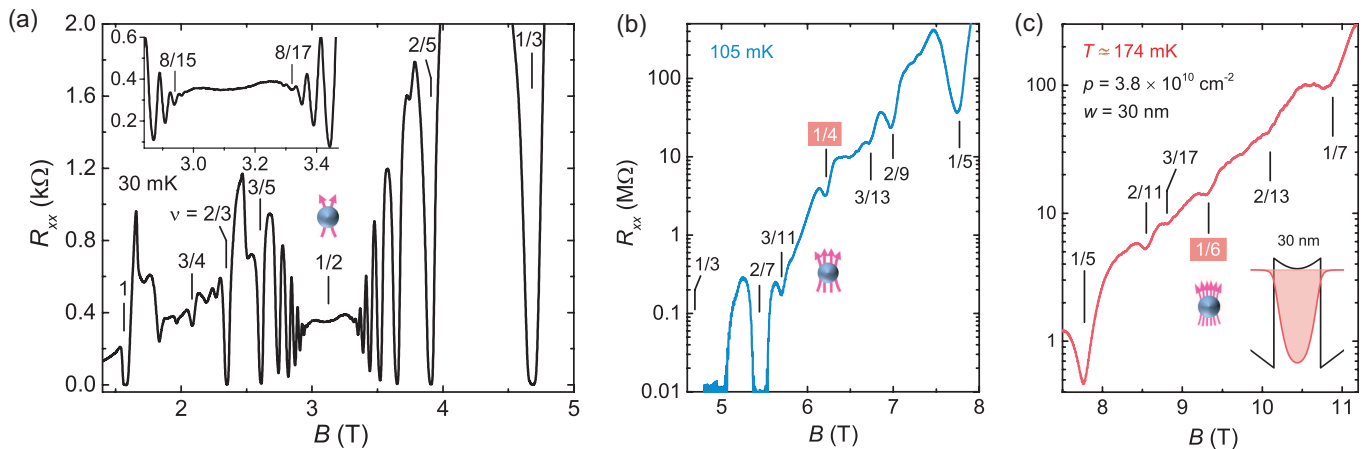


FIG. 1. Magneto-transport data for 2D holes confined to a 30-nm-wide GaAs quantum well in different filling factor ranges: (a) $1 > \nu > 1/3$, (b) $1/3 > \nu > 1/5$, and (c) $1/5 > \nu > 1/7$. Traces in (a) are shown in a linear scale, with k Ω as units of R_{xx} . Traces in (b) and (c) are shown with a \log scale for R_{xx} and in units of M Ω . The B positions of several fractional filling factors are marked with black vertical lines. Inset in (a): An enlarged version of the R_{xx} vs B near $\nu = 1/2$. Inset in (c): The self-consistently calculated hole charge distribution (red) and potential (black).

over liquid states. Similar phenomena were also reported in other materials such as AlAs [16, 17], ZnO [18], and bilayer graphene [19]. With recent advancements in the quality of GaAs 2DHSs [43, 44], many exotic FQHSs, likely emerging from composite fermion (CF) interaction and pairing induced by LLM, were observed at *even-denominator* fillings in the lowest LL [38–40].

Here we report the observation of numerous developing FQHSs in the lowest LL of ultrahigh-quality GaAs 2DHSs at *even-denominator* fillings $\nu = 1/6$ and $1/4$, and at odd-denominator fillings that follow the Jain sequence of four-flux and six-flux CFs (${}^4\text{CFs}$ and ${}^6\text{CFs}$). These states closely compete with pinned WC states which are dominant at $\nu < 1/3$. Our observations highlight the unexpected robustness of Jain FQHSs at extremely small fillings in the presence of severe LLM. They also suggest that, with sufficiently large LLM, the ${}^6\text{CFs}$ at $\nu = 1/6$ may undergo a pairing instability and condense into a non-Abelian FQHS, similar to what was recently reported at $\nu = 1/4$ [40, 41].

II. EXPERIMENTAL DETAILS

We studied an ultrahigh-quality 2DHS confined to a 30-nm-wide GaAs quantum well (QW) grown on a GaAs (001) substrate by molecular beam epitaxy. The 2DHS has a density of $3.8 \times 10^{10} \text{ cm}^{-2}$ and a low-temperature (0.03 K) record-high mobility of $18 \times 10^6 \text{ cm}^2/\text{Vs}$. The exceptionally high mobility was achieved by optimizing the growth chamber vacuum integrity and the purity of the source materials [45], as well as an optimized stepped-barrier design [43, 44]. We performed our experiments on $4 \times 4 \text{ mm}^2$ van der Pauw geometry samples cleaved from 2-inch GaAs wafers, and with alloyed In:Zn contacts at

the four corners and side midpoints. The samples were cooled in a dilution refrigerator and magneto-transport measurements were performed using low-frequency, lock-in amplifier techniques. A small excitation current of $I < 0.5 \text{ nA}$ was used for measuring the resistance of insulating phases to avoid self-heating and nonlinear I - V effect.

III. MAGNETO-TRANSPORT DATA

A. Developing fractional quantum Hall states at small ν

Figure 1(c) highlights our main findings: We observe numerous developing FQHSs on the flanks of $\nu = 1/6$ at odd-denominator fillings $\nu = 1/7, 2/13, \text{ and } 1/5, 2/11, 3/17$, evinced by sharp R_{xx} minima superimposed on a highly-insulating background. These states can be interpreted as Jain-sequence states (i.e., integer QHSs) of ${}^6\text{CFs}$ [at $\nu = n/(6n \pm 1)$, $n = 1, 2, 3$]. Remarkably, our data also exhibit a reasonably sharp R_{xx} minimum at $\nu = 1/6$, suggesting the emergence of an *even-denominator* FQHS, likely stabilized by the residual interaction and pairing of ${}^6\text{CFs}$. The observation of developing, even- and odd-denominator FQHSs at such small fillings is surprising because our 2DHS experiences severe LLM ($\kappa \simeq 6$ near $\nu = 1/6$), and large κ generally favors WC states over FQH liquid states at small ν [15, 16, 36].

At lower magnetic fields, we observe a developing even-denominator FQHS at $\nu = 1/4$, flanked by numerous FQHSs at odd-denominator fillings $\nu = 1/5, 2/9, 3/13, \text{ and } 1/3, 2/7, 3/11$ [Fig. 1(b)]. These observations are consistent with what was reported in ultrahigh-quality 2DHSs very recently [40], and the $\nu = 1/4$ FQHS is believed to emerge from the ${}^4\text{CF}$ pairing induced by sub-

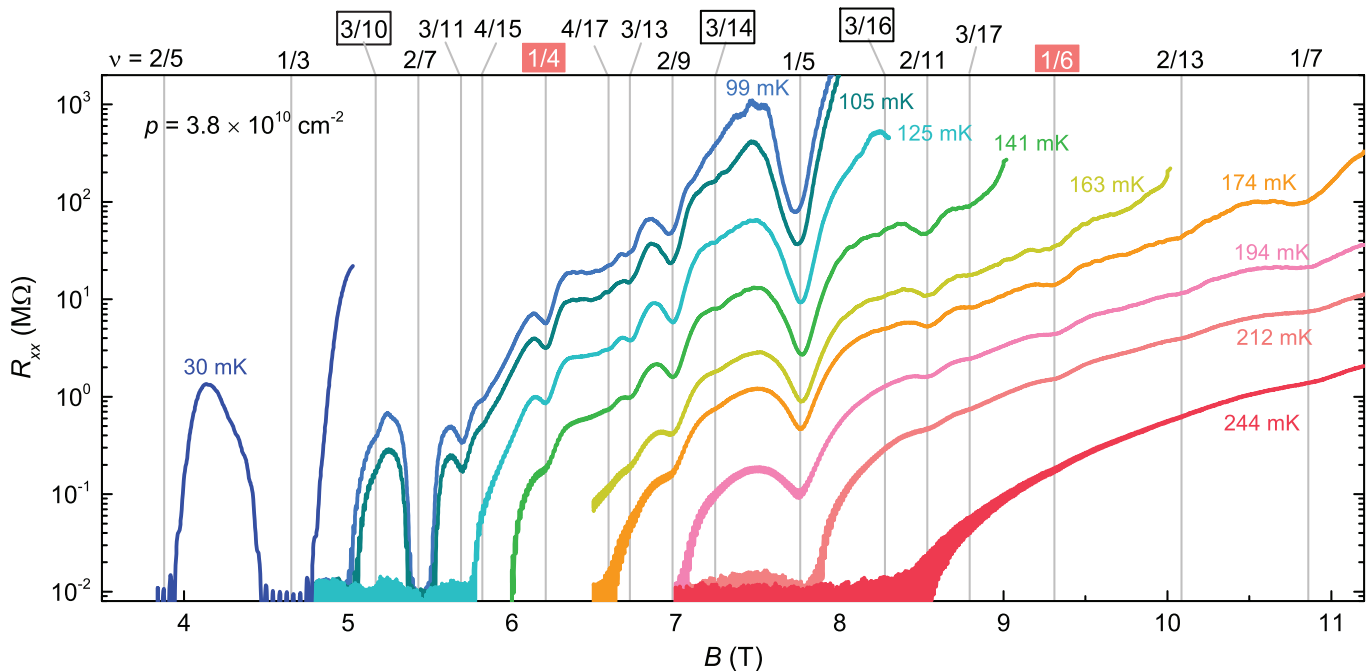


FIG. 2. R_{xx} vs B traces for $\nu \leq 2/5$ taken at different temperatures. The vertical lines mark the B positions of fractional filling factors as indicated on the top axis.

stantial LLM [41]. The odd-denominator FQHSs on the flanks of $\nu = 1/4$ can be interpreted as Jain-sequence states of ${}^4\text{CF}$ [$\nu = n/(4n \pm 1)$, $n = 1, 2, 3$]. It is noteworthy that the data shown in Figs. 1(b) and 1(c) were taken at elevated temperatures of $T \simeq 105$ mK and $\simeq 174$ mK, respectively, so that the 2DHS was less insulating (less resistive) and R_{xx} could be measured reliably. Figure 1(a) shows a trace measured at the base temperature $T \simeq 30$ mK for $1 > \nu > 1/3$. Near $\nu = 1/2$, the sample exhibits a smooth, shallow minimum, consistent with a compressible CF Fermi sea ground state at $\nu = 1/2$ [46]. The $\nu = 1/2$ minimum is flanked by numerous Jain-sequence FQHSs of two-flux CFs (${}^2\text{CFs}$) at $\nu = n/(2n \pm 1)$ ($n = 1, 2, \dots, 8$). We also observe a developing, exotic FQHS at $\nu = 3/4$ which can be interpreted as an even-denominator FQHS of ${}^2\text{CFs}$ arising from the CF-CF interaction and pairing in the half-filled, excited CF LL [38, 39].

In Fig. 2, we present R_{xx} vs B traces for $\nu < 2/5$ taken at different temperatures. FQHSs are fully developed at $\nu = 2/5, 1/3$, and $2/7$, evinced by vanishing R_{xx} and flat Hall plateaus quantized at $R_{xy} = h/\nu e^2$; see Fig. 8 in Appendix A for Hall data. Between these fully developed FQHSs, i.e., in filling ranges $2/5 > \nu > 1/3$ and $1/3 > \nu > 2/7$, as well as at higher B ($\nu < 2/7$), the data clearly reveal an insulating behavior: The R_{xx} values are extremely high (> 1 M Ω) at low temperatures and sharply decrease with increasing temperature. Such insulating phases were first reported in GaAs 2DESs for $\nu < 1/5$ and $2/9 > \nu > 1/5$ [7–12], and are believed to signal the formation of pinned WC phases. In systems

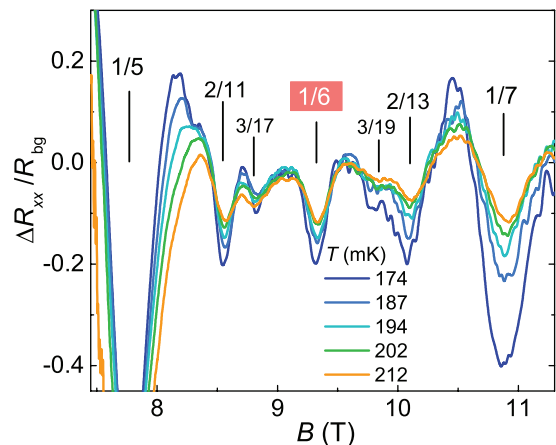


FIG. 3. $\Delta R_{xx}/R_{bg}$ vs B traces at different temperatures, where ΔR_{xx} represents the resistance after subtracting a smooth, increasing background R_{bg} . This background is estimated using a Savitzky-Golay filter with a 1 T window applied to R_{xx} vs B . We observe sharp R_{xx} minima at $\nu = 1/5, 2/11, 3/17, 2/13$, and $1/7$. The strengths of these minima weaken as ν is approaching $1/6$, and also weaken with increasing T , consistent with what is expected for Jain-sequence FQHSs. Additionally, we observe a sharp minimum at $\nu = 1/6$, closely resembling those observed at Jain-sequence fillings and suggesting a developing FQHS at $\nu = 1/6$.

with large LLM like our GaAs 2DHS, experiments [13–19] and theoretical calculations [36] show that the onset

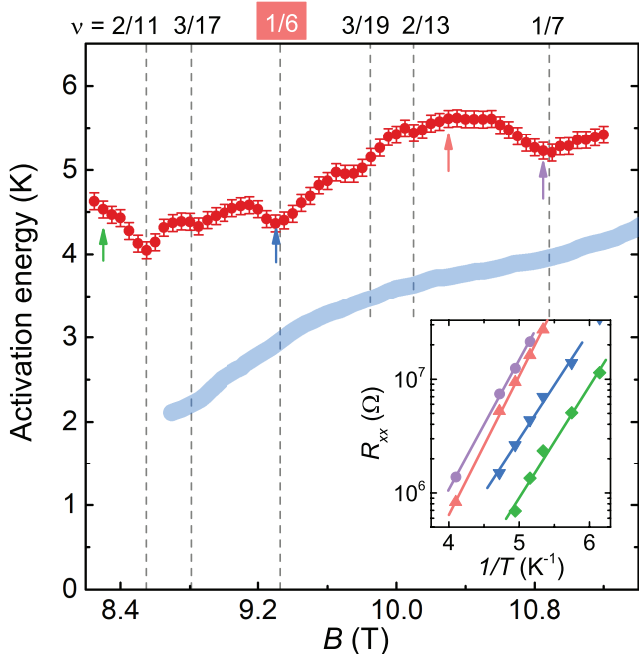


FIG. 4. Activation energy vs B for R_{xx} data shown in Fig. 2 at extremely small fillings $\nu < 1/5$. The blue curve represents theoretical values of the CF WC defect formation energy reported in Ref. [48]. Inset shows R_{xx} vs $1/T$ Arrhenius plots at various B , each color coded according to the B values marked by the arrows in the main figure.

of insulating phases moves to larger fillings, near $\nu = 1/3$, consistent with our data in Fig. 2.

Note in Fig. 2 that the R_{xx} minima at $\nu = 1/6$ and $1/4$ are observed in a reasonably wide range of temperatures (163 ~ 194 mK for $\nu = 1/6$, and 99 ~ 125 mK for $\nu = 1/4$). With further increase in T , these minima turn into inflection points and eventually disappear. Such evolution of R_{xx} minima at $\nu = 1/4$ and $1/6$ with increasing T is very similar to what is observed at Jain-sequence odd-denominator fillings flanking $\nu = 1/4$ and $1/6$, supporting that they are indeed developing FQHSs. We also note that between the $n = 1$ and $n = 2$ Jain-sequence states, instead of a smooth R_{xx} dome, our sample exhibits inflection points at $\nu = 3/10$, $3/14$, and $3/16$, also evinced by peaks in d^2R_{xx}/dB^2 vs B ; see Fig. 10 in Appendix B for more details. These features could be precursors of developing even-denominator FQHSs of ${}^4\text{CFs}$ and ${}^6\text{CFs}$, analogous to the exotic $\nu = 3/4$ FQHS [38, 39].

In order to more clearly reveal the R_{xx} minima and inflection points riding on the insulating phases for $\nu \lesssim 1/5$, Fig. 3 presents $\Delta R_{xx}/R_{bg}$ vs B traces at various temperatures. Here, ΔR_{xx} represents the resistance after subtracting a smooth, increasing background R_{bg} ; see Fig. 9 and Appendix B for details. We observe sharp $\Delta R_{xx}/R_{bg}$ minima at $\nu = 1/5$, $2/11$, $3/17$, $2/13$, and $1/7$. The strength of these minima weakens as ν is approaching $1/6$, and also weakens with increasing T , consistent

with what is expected for Jain-sequence FQHSs. Additionally, we observe a sharp minimum at $\nu = 1/6$, closely resembling those observed at Jain-sequence fillings and suggesting a developing FQHS at $\nu = 1/6$.

B. Activation energy of Wigner crystal states

Next, we study the WC states that compete with FQHSs at extremely small fillings. In Fig. 4, we present activation energy (E_A) data deduced from the relation $R_{xx} \propto e^{E_A/2kT}$ as a function of B . The inset in Fig. 4 shows representative R_{xx} vs $1/T$ Arrhenius plots and the linear fits whose slopes give the value of E_A at a given B . The magnitude of E_A is associated with the defect formation energy of a WC. Numerical calculations indicate that, at small fillings ($\nu < 1/5$), a WC formed by ${}^4\text{CFs}$ has lower energy than the conventional Hartree-Fock electron crystal [47], and that the lowest-energy *intrinsic* defect in this ${}^4\text{CF}$ WC is a hyper-correlated quantum bubble defect [48]. Recent measurements [49] on ultrahigh-quality 2DESs indeed show E_A values closely matching with that expected for an ideal ${}^4\text{CF}$ WC with no disorder, consistent with the fact that the WC domains in these samples are estimated to contain $\simeq 1000$ electrons [50]. Experiments on modest quality GaAs 2DESs [51, 52] and ultrahigh-quality 2DESs in the dilute limit [49] show somewhat smaller values of E_A compared to calculations. These discrepancies were attributed to the effects of disorder and LLM which are generally believed to lower E_A . Surprisingly, our 2DHS exhibits E_A significantly *larger* than what was reported for 2DESs at a similar density of $4.4 \times 10^{10} \text{ cm}^{-2}$ [49], even though the LLM parameter κ for our 2DHS ($\kappa \simeq 5$) is about seven times larger than κ for the 2DES ($\kappa \simeq 0.7$). The E_A values for our 2DHS are even larger than the calculated values reported in Ref. [48]; see the blue curve in Fig. 4. The anomalously large measured E_A suggests that the nature of the WC and/or the lowest-energy intrinsic defect of the WC in our ultrahigh-quality 2DHS might be of a different type.

IV. DISCUSSION

A. Estimate of Landau level mixing parameter κ for GaAs 2DHSs

It is noteworthy that, unlike GaAs 2DESs whose LLs are linear in energy as a function of B , GaAs 2DHSs have highly nonlinear LLs because of the heavy-hole light-hole coupling [32, 33]; see e.g. Fig. 5(a). The complex LL diagram exhibits numerous LL crossings that can be tuned to coincide with the Fermi energy (E_F), giving rise to exotic interaction phenomena [53–57]. On the other hand, this nonlinearity make a quantitative evaluation of the cyclotron energy and LLM parameter κ more challenging [40, 56]. In addition, the heavy-hole light-hole

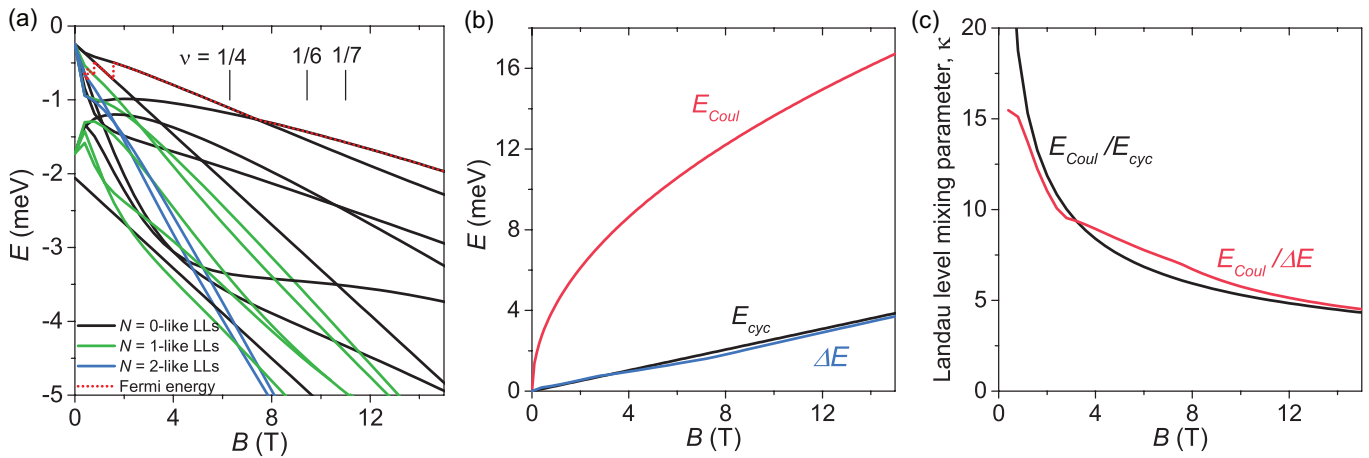


FIG. 5. (a) Calculated energy E vs B Landau level diagram. Different LLs are color-coded according to their dominant orbital component in the field range $4 < B < 12$ T where competing FQHSs and WC states are observed. The red dotted line traces the Fermi energy E_F . LLs with energy much lower than E_F are not shown for simplicity. (b) Coulomb energy E_{Coul} , cyclotron energy E_{cyc} , and the separation ΔE between the topmost $N = 0$ -like and $N = 1$ -like LLs for our 2DHS as a function of B . (c) Landau level mixing parameters according to two different definitions.

and spin-orbit couplings in holes render hole LLs multi-component, making the orbital quantum number N not a good quantum number for a hole LL [33, 58]. This adds complexity to the definition of cyclotron energy and κ . In the remainder of this article, we present LL calculations for our 2DHS to shed light on the estimation and effect of κ in the extreme quantum limit.

We calculated the E vs B LL diagram for our 2DHS, using the multiband envelope function approximation and the 8×8 Kane Hamiltonian [33]. For simplicity, in Fig. 5(a), we only show the topmost LLs which are most relevant to our study. We expand these LLs in a basis of four spinors, each of which can be described by a spin quantum number ($s_z = \pm 1/2$ or $\pm 3/2$) and an orbital quantum number ($N = 0, 1, 2, \dots$); see Appendix E for detailed results of our calculations. The LLs in Fig. 5(a) are color-coded based on N of the leading spinor component in the range $4 < B < 12$ T. Figure 5(b) shows the different energy scales in the extreme quantum limit: (i) Coulomb energy $E_{Coul} = e^2/(4\pi\epsilon l_B) \propto \sqrt{B}$, where $l_B = \sqrt{\hbar/eB}$ is the magnetic length; (ii) cyclotron energy $E_{cyc} = \hbar e B/m_0^* \propto B$, where $m_0 = 0.45$ (in units of free electron mass) is the calculated band mass at $B = 0$; and (iii) ΔE , defined as the separation between the topmost $N = 0$ -like LL and $N = 1$ -like LL in Fig. 5(a) [59].

We find that in Fig. 5(b), E_{cyc} and ΔE are close throughout the range of B . Such an agreement is surprising because the former is from a $B = 0$ energy band calculation while the latter is extracted from the LL calculations in large B where the LLs are complex and nonlinear. It is worth noting that the simple picture of $E_{cyc} = \hbar e B/m_0^*$ has been used to estimate κ for GaAs 2DHSs in the past [14, 15]. A reasonably good agreement on κ vs ν WC quantum melting phase diagram

near $\nu = 1/3$ was found between experimental results on GaAs 2DHSs [15] and calculations [36]. As we will discuss later, our data points are also consistent with the calculated phase diagram; see Fig. 6. The $E_{cyc} \simeq \Delta E$ we find in Fig. 5(b) may explain these agreements.

B. Competition between FQHSs and WC states: Role of LLM

The fact that E_{Coul} is significantly larger than E_{cyc} and ΔE highlights the importance of LLM. The ratios E_{Coul}/E_{cyc} and $E_{Coul}/\Delta E$ offer two estimates for κ in the extreme quantum limit [Fig. 5(c)]. They both yield $9 \gtrsim \kappa \gtrsim 5$ for $4 < B < 12$ T [60]. The large $\kappa \simeq 5$ near $\nu = 1/7$ in our 2DHS is about six to ten times larger than κ of GaAs 2DESs where a developing $\nu = 1/7$ FQHS was reported [26–29].

Figure 6 shows WC quantum melting phase diagrams, with LLM parameter κ and ν for axes. The solid lines in panels (a) and (c) represent calculated phase boundaries between the WC and liquid states from Ref. [36]. The red and black circles represent two estimates of κ for our 2DHS shown in Fig. 5. Numerical calculations [36] indicate that, while the $\nu = 1/3$ FQHS is very robust to LLM and survives even for $\kappa > 18$ [see Fig. 6(a)], the $\nu = 1/5$ FQHS gives way to a WC phase for $\kappa \gtrsim 10$ [Fig. 6(c)]. This is consistent with experimental results [15, 16]; also see Figs. 6(a) and (c). Although there are no existing theories for the role of LLM at even smaller fillings near $\nu = 1/7$, based on the trend discussed above, one would expect that FQHSs are more fragile at large κ and would lose the competition to WC phases. Therefore, our observation of numerous odd- and even-denominator FQHSs at extremely small fillings, e.g. at $\nu = 1/7$ and

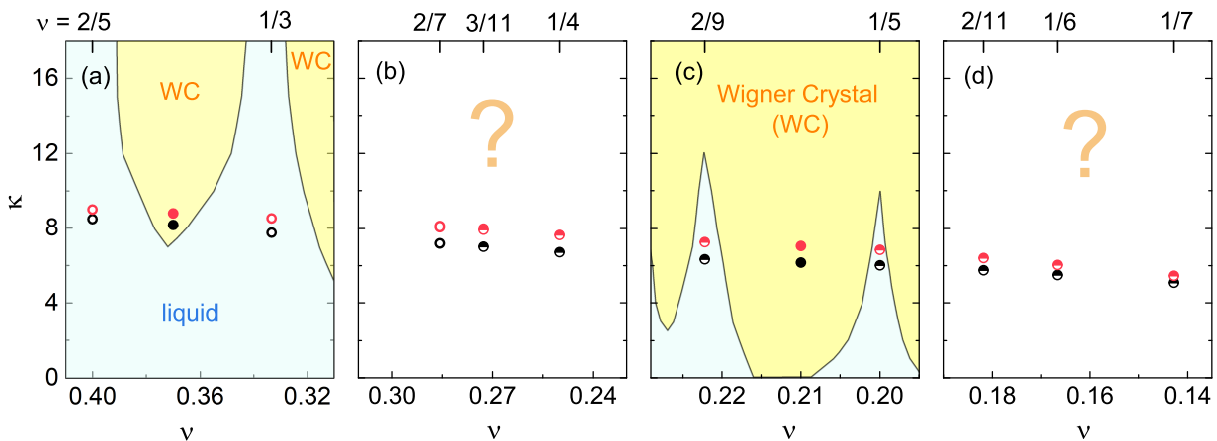


FIG. 6. WC quantum melting phase diagrams, with LLM parameter κ and ν for axes. Panels (a) and (c) present the calculated phase diagrams near $\nu = 1/3$ and $1/5$, respectively [36]. The yellow and blue regions indicate the predicted WC and liquid phases. So far, there have been no theoretical calculations for the ν ranges shown in panels (b) and (d), where a close competition between FQHSs and WC states is observed in our samples. The open and solid circles denote the liquid and WC phases, respectively. The half-filled circles denote developing FQHSs in close competition with WC phases. The red and black circles represent two estimates of κ for our 2DHS, as discussed in the text and Fig. 5(c).

$1/6$, in the presence of severe LLM ($\kappa \simeq 5$) is surprising and calls for new theories and numerical calculations.

Our data points in Figs. 6(a, c) agree well with the calculated phase diagrams. As shown in Fig. 6(a), we observe fully developed FQHSs at $\nu = 1/3$ and $2/5$ (open circles), and a reentrant insulating phase between $\nu = 1/3$ and $2/5$ (solid circles), consistent with the expectation of a LLM-induced WC phase flanked by robust FQHSs at $\nu = 1/3$ and $2/5$.

For $1/5 \lesssim \nu \lesssim 2/9$, we observe developing FQHSs at $\nu = 1/5$ and $2/9$ [half-filled circles in Fig. 6(c)], i.e., sharp R_{xx} minima that rise with decreasing T , signaling the close competition between FQHSs and WC states. Such a competition is also revealed by the calculated phase diagram shown in Fig. 6(c): Based on our estimates of κ for the 2DHS, theory predicts that FQHSs only win in a narrow range of ν near $1/5$ and $2/9$, while WC states prevail elsewhere. Therefore, in real systems like our 2DHS, a small variation of ν caused by a minuscule density inhomogeneity or disorder can lead to the formation of WC domains and prevent the percolation of the FQH liquid. This explains why in our data the R_{xx} minima do not reach zero at $\nu = 1/5$, $2/9$ and also other fractional ν where FQHSs emerge in the WC-dominated regime.

For the ν ranges shown in Figs. 6(b) and (d), we observe a fully developed FQHS at $\nu = 2/7$ and numerous developing FQHSs in close competition with WC states. However, no theoretical calculations exist for these ν ranges.

C. Comparison with GaAs and AlAs 2DESs

Next, we compare our results with recent findings in ultrahigh-quality GaAs and AlAs 2DESs at extremely small $\nu < 1/5$ [17, 28, 29]. GaAs 2DESs are considered hallmark platforms in quantum Hall physics thanks to their record-high mobility [45, 61]. In state-of-the-art GaAs 2DESs, developing Jain-sequence FQHSs of ${}^6\text{CFs}$ are seen on the flanks of $\nu = 1/6$, at $\nu = 1/7, 2/13, 3/19, 3/17, 2/11$, and $1/5$ [29]. A sharp R_{xx} minimum at $1/6$, signaling the emergence of a developing FQHS, is seen only when the 2DES is confined to a relatively wide QW, and has a single-layer, albeit thick, charge distribution [29]. Similar to the $\nu = 1/6$ FQHS in our 2DHS, the $\nu = 1/6$ FQHS in GaAs 2DESs likely arises from the pairing of ${}^6\text{CFs}$ [62]. Rather than LLM, it is the substantial electron layer thickness that softens the electron-electron Coulomb repulsion and facilitates CF pairing.

AlAs 2DESs also experience severe LLM at small ν thanks to their large effective mass and small dielectric constant compared to GaAs 2DESs. In AlAs 2DESs, signatures of developing FQHSs were very recently observed at $\nu = 1/7$ and $2/11$ with $\kappa \simeq 4$ [17]. These findings qualitatively align with our data, although our 2DHS also shows hints of more high-order Jain-sequence FQHSs, e.g., at $\nu = 3/17$ and $2/13$. Unlike the emerging FQHSs at $\nu = 1/4$ and $1/6$ in our 2DHSs, AlAs 2DESs do not show any FQHS feature at these even-denominator fillings. At first sight, the absence of $\nu = 1/4$ and $1/6$ FQHSs in AlAs might appear to contradict our interpretation that these states arise from the pairing of ${}^4\text{CFs}$ and ${}^6\text{CFs}$ induced by LLM. However, several differences between the systems should be noted: (i) AlAs 2DESs

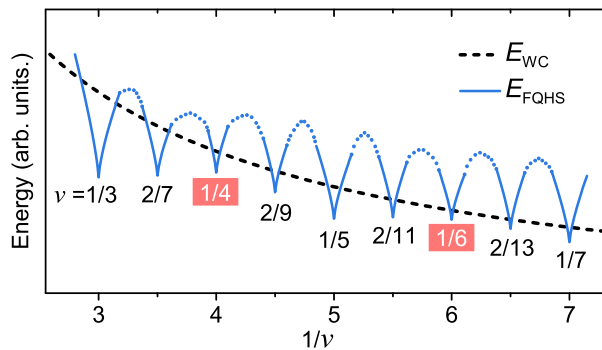


FIG. 7. Schematic diagram showing the energies of WC and FQHSs vs $1/\nu$ for $\nu \lesssim 1/3$. While the energy of WC is expected to be a smooth function of $1/\nu$ [2, 47], the energies of FQHSs exhibit downward cusps at proper fractional ν , and can dip below the WC energy so that the WC could be reentrant on the flanks of a FQHS. This explains our observation of (developing) FQHSs at odd- and even-denominator fillings flanked by WC states (Fig. 2). For clarity, we only show the energies of FQHSs at $\nu = 1/n$ and $2/n$, where n is an integer.

have highly anisotropic Fermi contours, whereas GaAs 2DHSs at low densities have nearly isotropic Fermi contours. (ii) As discussed earlier, the LLs of GaAs 2DHSs are complex and nonlinear; on the other hand, the AlAs 2DESs have simple LLs. (iii) The quality of GaAs 2DHSs is generally superior to that of AlAs 2DESs, as reflected by the order-of-magnitude larger mobility of the GaAs 2DHSs [43, 44] compared to AlAs 2DESs [63].

D. FQHSs vs CF Fermi seas at $\nu = 1/4$ and $1/6$

Another potentially competitive ground state at $\nu = 1/6$ (and $1/4$) is a metallic Fermi sea of ${}^6\text{CF}$ s (${}^4\text{CF}$) at zero *effective* magnetic field. One might take the R_{xx} minima at $\nu = 1/6$ and $1/4$ as evidence for a CF Fermi sea at these fillings, similar to what is observed near $\nu = 1/2$. While such an interpretation is also novel as there has been no experimental or theoretical evidence for such a phase deep in the low-filling, insulating, WC regime, we argue that it is unlikely that the R_{xx} minima we observe at $\nu = 1/6$ and $1/4$ are indications of Fermi seas of ${}^4\text{CF}$ s and ${}^6\text{CF}$ s, but rather strongly favor developing FQHSs. First, our temperature dependence data reveal that the R_{xx} minima at $\nu = 1/4$ and $1/6$ highly resemble those observed at surrounding odd-denominator, Jain-sequence fillings where developing FQHSs are expected. Second, theoretical calculations suggest that substantial LLM can induce ${}^4\text{CF}$ pairing at $\nu = 1/4$, and thereby favor a FQHS over a CF Fermi sea [41]. Similar physics may be extended to $\nu = 1/6$. Third, the sharp R_{xx} minimum observed in the WC regime at $\nu = 1/6$ (and $1/4$) indicates that the $\nu = 1/6$ (and $1/4$) state is flanked by WC states. This strongly favors the interpre-

tation of FQHS over ${}^6\text{CF}$ (${}^4\text{CF}$) Fermi sea: The energies of FQHSs show downward cusps as a function of ν , and can dip below the WC energy (see Fig. 7) so that the WC could be reentrant on the flanks of a FQHS [8, 47, 64]. On the other hand, the energies of both CF Fermi sea and WC states are smooth functions of ν , and thus one would expect only a single transition between these two states. It is also worth noting that the observation of Jain-sequence FQHSs around a given even-denominator filling does not necessarily indicate the presence of a CF Fermi sea at that filling. Indeed, a FQHS at $\nu = 1/2$ flanked by numerous Jain-sequence FQHSs is well established in 2DESs confined to wide GaAs QWs [67, 68].

V. SUMMARY

Our observation of numerous developing FQHSs at extremely small, even- and odd-denominator ν competing with WC states highlights the rich physics in the lowest LL of ultrahigh-quality GaAs 2DHSs. The robustness of FQHSs in the presence of LLM is surprising, and should inspire further theoretical calculations. Also puzzling are the anomalously large activation energies we measure in the WC regime (Fig. 4); they suggest that the WC intrinsic defects may be different in a 2D system with severe LLM.

ACKNOWLEDGMENTS

We acknowledge support by the National Science Foundation (NSF) (Grant No. DMR 2104771) for measurements, the U.S. Department of Energy (DOE) Basic Energy Sciences (Grant No. DEFG02-00-ER45841) for sample characterization, and the National Science Foundation (NSF) (Grant No. ECCS 1906253), the Eric and Wendy Schmidt Transformative Technology Fund, and the Gordon and Betty Moore Foundation's EPiQS Initiative (Grant No. GBMF9615 to L.N.P.) for sample fabrication. Our measurements were partly performed at the National High Magnetic Field Laboratory (NHMFL), which is supported by the NSF Cooperative Agreement No. DMR 2128556, by the State of Florida, and by the DOE. This research is funded in part by QuantEmX grants from Institute for Complex Adaptive Matter and the Gordon and Betty Moore Foundation through Grant No. GBMF9616 to C. W. and S. K. S. We thank A. Bangura, R. Nowell, G. Jones, and T. Murphy at NHMFL for technical assistance, and P. T. Madathil, A. C. Balram and J. K. Jain for illuminating discussions.

Appendix A: Hall data

Figure 8(b) shows Hall resistance (R_{xy}) as a function of B for the 2DHS discussed in the main text. In Fig. 8(a), we present R_{xx} data for the same range of B . We

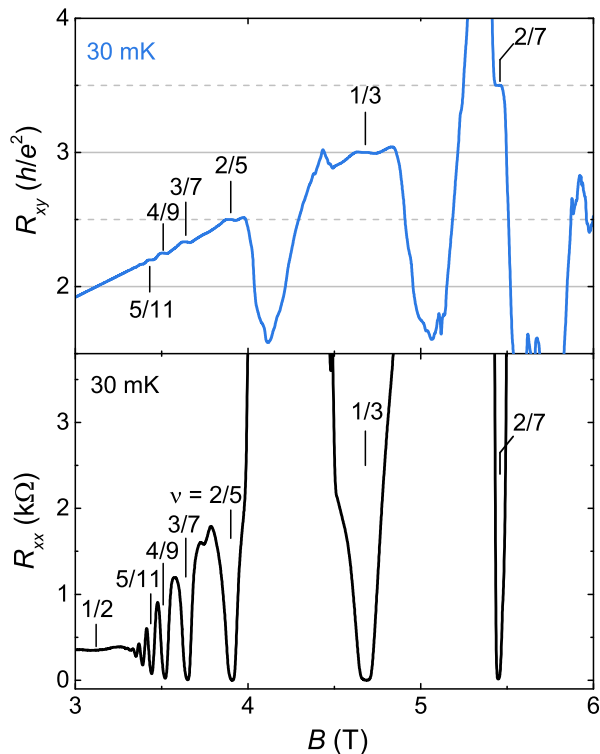


FIG. 8. **Hall data.** (a) Longitudinal resistance (R_{xx}) and (b) Hall resistance (R_{xy}) vs B traces measured with $I = 100$ nA at $T \simeq 30$ mK. Different LL fillings are marked by vertical lines.

observe FQHSs at $\nu = 1/3, 2/5, 3/7, \dots$, and also at $\nu = 2/7$, evinced by deep R_{xx} minima and quantized Hall plateaus. We note that in the ranges $\nu < 2/7$, $1/3 > \nu > 2/7$, and $2/5 > \nu > 1/3$, where the 2DHS is highly insulating, the R_{xy} trace significantly deviates from the linear trend because of the effect of R_{xx} mixing. This is a well-known problem, and manifests itself in the low- ν regime where there is a close competition between WC states and FQHSs [26, 65, 66]. Although flanked by insulating phases, the FQHSs at $\nu = 1/3$ and $2/7$ are fully developed at $T \simeq 30$ mK, with R_{xx} reaching zero and flat R_{xy} plateaus quantized at $3h/e^2$ and $7h/2e^2$, respectively.

Appendix B: Resistance background subtraction and d^2R_{xx}/dB^2 data at small ν

In order to better visualize the FQHS features in R_{xx} amidst the dominant insulating behavior caused by the competing WC states, we extract the oscillatory component (ΔR_{xx}) of the R_{xx} data. Here $\Delta R_{xx} = R_{xx} - R_{bg}$ is defined as the resistance after subtracting a smooth, increasing background R_{bg} . As we show in Fig. 3, sharp minima are revealed in the $\Delta R_{xx}/R_{bg}$ vs B traces. Figure 9 displays the raw R_{xx} vs B traces (black) and their

corresponding R_{bg} (green) at different temperatures. The resistance background R_{bg} , contributed by the insulating phase, is estimated using a Savitzky-Golay filter with a 1 T window applied to R_{xx} vs B data. This window size captures the main trend of the slowly varying part of R_{xx} while minimizing artifacts.

Another effective method to extract FQHS features from highly insulating R_{xx} data is to calculate the second derivative, d^2R_{xx}/dB^2 . Figure 10 shows R_{xx} (top panels) and d^2R_{xx}/dB^2 (bottom panels) as a function of inverse filling $1/\nu$ for different temperatures and ranges of $1/\nu$. At $\nu = 1/3$ and $2/7$, FQHSs are fully developed, evinced by vanishing R_{xx} spanning a range of $1/\nu$ and zero d^2R_{xx}/dB^2 flanked by two peaks; see yellow-shaded part in Fig. 10(a). At small ν deep in the insulating regime where WC states are dominant, a developing FQHS manifests itself as a minimum or an inflection point in R_{xx} with a maximal curvature and therefore exhibits a peak in d^2R_{xx}/dB^2 . In Fig. 10, we observe clear R_{xx} minima superimposed on a highly insulating background at odd-denominator fillings $\nu = 3/11, 3/13, 2/9, 1/5, 2/11, 3/17$, and $1/7$, signaling the developing Jain-sequence states of four-flux and six-flux composite fermions (${}^4\text{CFs}$ and ${}^6\text{CFs}$). Clear R_{xx} minima are also seen at even-denominator fillings $\nu = 1/4$ and $1/6$, suggesting developing FQHSs, likely emerging from the pairing instability of ${}^4\text{CFs}$ and ${}^6\text{CFs}$. In addition, we also see inflection points at certain fillings, including odd-denominator fillings, consistent with high-order Jain-sequence states of ${}^4\text{CFs}$ ($\nu = 4/15$ and $4/17$) and ${}^6\text{CFs}$ ($\nu = 2/13, 3/19$, and $4/25$), and even-denominator fillings at $\nu = 3/10, 3/14, 3/16$, and $3/20$.

Appendix C: Summary of developing FQHSs at extremely small ν

In Table. I, we list all the filling factors ν at which FQHS features in R_{xx} and/or R_{xy} are observed in our 2DHS. States denoted in boldface are fully developed FQHSs, well established by the observation of vanishing R_{xx} and quantized R_{xy} plateaus. States represented in regular font indicate developing FQHSs, evinced by discernible R_{xx} minima on top of an insulating background. States shown in italic denote observed inflection points in R_{xx} . States at even-denominator fillings are highlighted in red. We map these hole LL fillings ν to CF Lambda level (ΛL) fillings [3] of ${}^4\text{CFs}$ and ${}^6\text{CFs}$. The odd-denominator, Jain-sequence FQHSs can be mapped to interger QHSs of ${}^4\text{CFs}$ and ${}^6\text{CF}$. Note that the states at even-denominator $\nu = 3/10, 3/14, 3/16$, and $3/20$ can all be mapped to a CF ΛL filling of $3/2$. These states likely emerge from the same mechanism as those observed at $\nu = 3/4$ and $3/8$, which can be interpreted as "next-generation" even-denominator FQHSs of CFs with ΛL filling of $3/2$ for two-flux CFs. [38, 39].

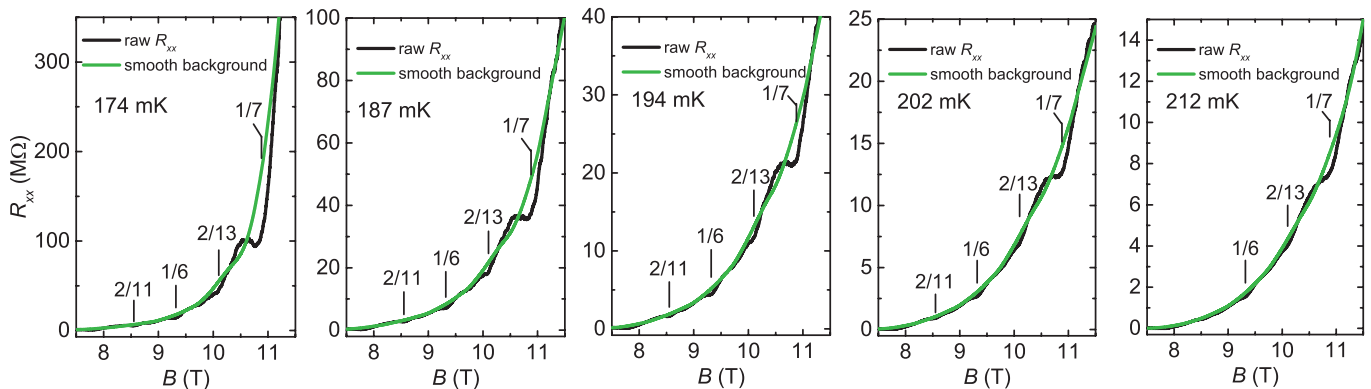


FIG. 9. **Resistance background subtraction.** Raw R_{xx} vs B traces (in black) and their corresponding smooth background (R_{bg} , in green) at different temperatures. R_{xx} clearly dips below R_{bg} at $\nu = 2/11, 1/6, 2/13,$ and $1/7$.

TABLE I. List of FQHSs observed in our 2DHS at $\nu \leq 1/3$. States denoted in boldface are fully developed FQHSs, well established by the observation of vanishing R_{xx} and quantized R_{xy} plateaus. States represented in regular font indicate developing FQHSs, evinced by discernible R_{xx} minima on top of an insulating background. States shown in italic denote observed inflection points in R_{xx} . States at even-denominator fillings are highlighted in red.

CF AL fillings	1	$3/2$	2	3	4	∞
${}^4\text{CF}$	1/3	<i>3/10</i>	2/7	3/11	<i>4/15</i>	<i>1/4</i>
	1/5	<i>3/14</i>	2/9	3/13	4/17	<i>1/4</i>
${}^6\text{CF}$	1/5	<i>3/16</i>	2/11	3/17		<i>1/6</i>
	1/7	<i>3/20</i>	<i>2/13</i>	<i>3/19</i>	<i>4/25</i>	<i>1/6</i>

Appendix D: Magneto-transport data for a different sample

In Fig. 11, we present R_{xx} data for a different sample measured at different temperatures. The 2DHS is confined to a 35-nm-wide quantum well, and has a hole density of $4.1 \times 10^{10} \text{ cm}^{-2}$. We observe qualitatively similar behaviors compared to the sample we discuss in the main text (see Fig. 2 of the main text): (i) The 2DHS shows an insulating behavior in the filling ranges $2/5 > \nu > 1/3$, $1/3 > \nu > 2/7$, and $\nu < 2/7$. (ii) Fully developed FQHSs are seen at $\nu = 1/3$ and $2/7$, evinced by vanishing R_{xx} . (iii) R_{xx} minima and inflection points superimposed on a highly insulating background are observed at odd-denominator fillings $\nu = n/(4n \pm 1)$ and $\nu = n/(6n \pm 1)$, where n are integers. These features are consistent with developing Jain-sequence FQHSs of ${}^4\text{CF}$ s and ${}^6\text{CF}$ s. (iv) At even-denominator fillings $\nu = 1/4$ and $1/6$, respectively, a R_{xx} minimum and an inflection point are observed, suggesting developing FQHSs. The R_{xx} minima and inflection points at $\nu = 2/11, 3/17, 1/6, 2/13,$ and $1/7$ are clearly revealed as sharp minima in $\Delta R_{xx}/R_{bg}$ in the inset of Fig. 11, where we present $\Delta R_{xx}/R_{bg}$ vs B at 175 mK. These observations demonstrate that the competing FQHSs and WC phases at small LL fillings we report in the main text are robust and reproducible phenomena in ultrahigh-quality 2DHSs.

Appendix E: Landau level calculations

We performed LL calculations using the multi-band envelope function approximation based on the 8×8 Kane Hamiltonian [33] for our 2DHS studied in the main text. The model also uses the axial approximation which neglects the effect of cubic anisotropy of the crystal structure. Figure 12(a) shows the calculated E vs B LL diagram. The LLs are nonlinear as a function of B and are not evenly spaced in E at a particular B because of the strong coupling between heavy-hole (HH) and light-hole (LH) subbands [33]. This implies that the cyclotron energy may not be well defined for GaAs 2DHSs.

The nonlinearity as a function of B is closely related to the fact that the hole LLs also have a more complex nature compared to electron LLs for a GaAs 2D electron system (2DES). Unlike the simple LLs for a GaAs 2DES that can be described by an orbital quantum number $N = 0, 1, 2, \dots$ and a spin quantum number $s = \pm 1/2$, for hole LLs N and s are not good quantum numbers. While the eigenstates at zero B (and in-plane wave vector $k_{\parallel} = 0$) are purely HH with $s = \pm 3/2$ or LH with $s = \pm 1/2$, the HH-LH coupling at $B > 0$ leads to eigenstates with mixed HH and LH components. Strictly speaking, the eigenstates in the accurate 8×8 Kane model have eight spinor components. However, for the hole states relevant here the weights of the additional four spinor components

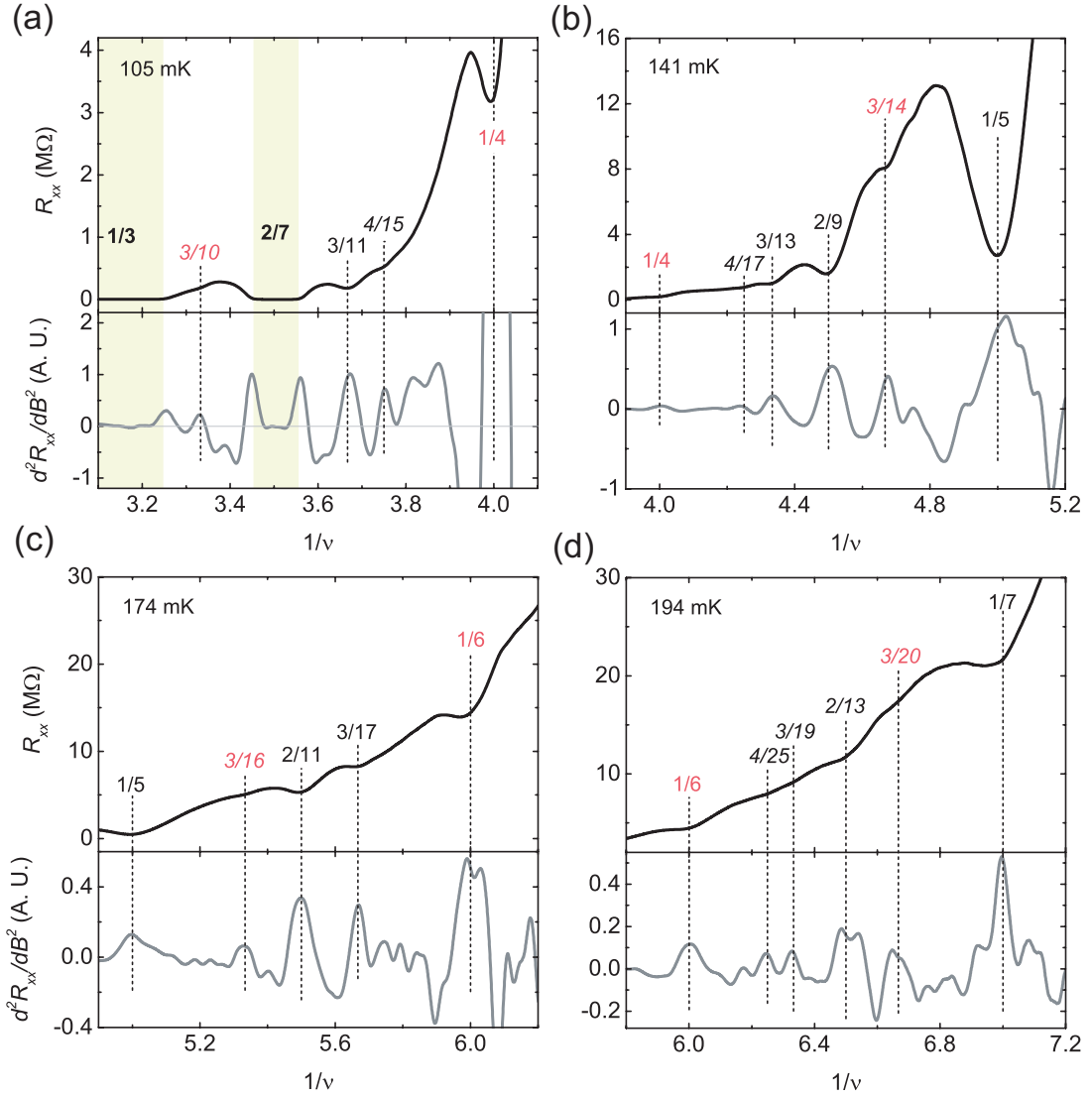


FIG. 10. **Evidence for developing FQHSs.** R_{xx} and $d^2 R_{xx}/dB^2$ for our 2DHS with density $3.8 \times 10^{10} \text{ cm}^{-2}$ are plotted as a function of inverse filling $1/\nu$ for different temperatures and ranges of $1/\nu$. Vertical dotted lines indicate the positions where developing FQHSs are observed, evinced by R_{xx} minima (or inflection points), and by sharp peaks in $d^2 R_{xx}/dB^2$.

are small relative to the HH and LH components, and they are therefore ignored in the following discussion.

We emphasize that the coupling and mixing of HH and LH components in a single LL is fundamentally different from the LL mixing (LLM) we discuss in the main text. The former is a consequence of HH-LH coupling in the single-particle picture (the single-particle eigenstates in a quantizing magnetic field are already a superposition of Landau harmonic oscillators), while the latter (LLM) is a many-body effect induced by the Coulomb interaction. LLM happens on top of what is already present due to HH-LH coupling. As we discuss next, in order to make quantitative estimates of the LLM parameter κ , we simplify the problem by expanding the hole LLs in a basis of four spinors and treating each hole LL as a single com-

ponent LL described by its leading spinor component.

Here we limit our analysis to the topmost LLs at high B [shown in Fig. 12(a) in black] which are most relevant to our study of correlated states at high B , and other LLs [shown in Fig. 12(a) in grey] that are further away from the Fermi energy are neglected for simplicity and clarity. In Fig. 12(b), we replot Fig. 4(a) of the main text, showing the most relevant LLs, color-coded according to their dominant orbital component in the field range $4 < B < 12$ T where competing FQHSs and WC states are observed.

Next, we discuss in detail how we determine the dominant orbital component for the LLs shown in Fig. 12(b). The LLs at $B > 0$ can be decomposed into a basis of four

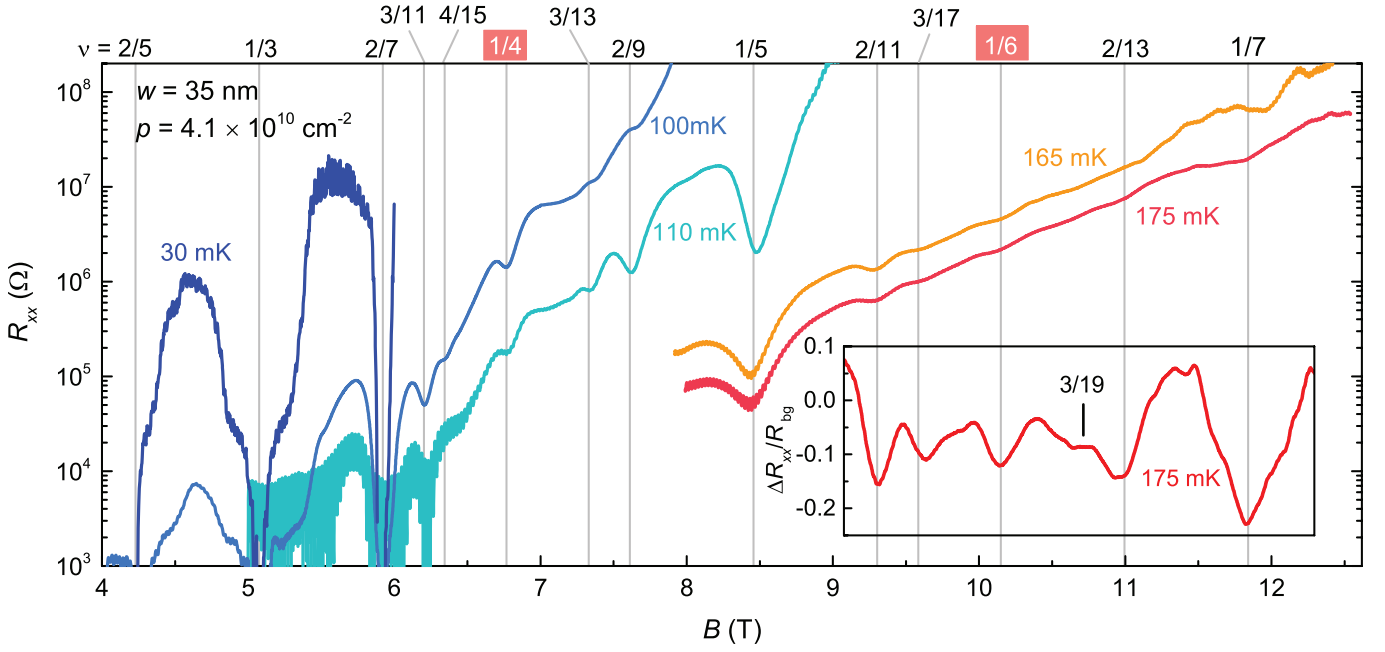


FIG. 11. **Magneto-transport data for a 35-nm-wide quantum well.** R_{xx} vs B traces measured with $I = 0.1$ nA at different temperatures. The vertical lines mark the B positions of fractional filling factors indicated on the top axis. Inset presents $\Delta R_{xx}/R_{bg}$ in the range $9 \lesssim B \lesssim 12.3$ T for $T \simeq 175$ mK.

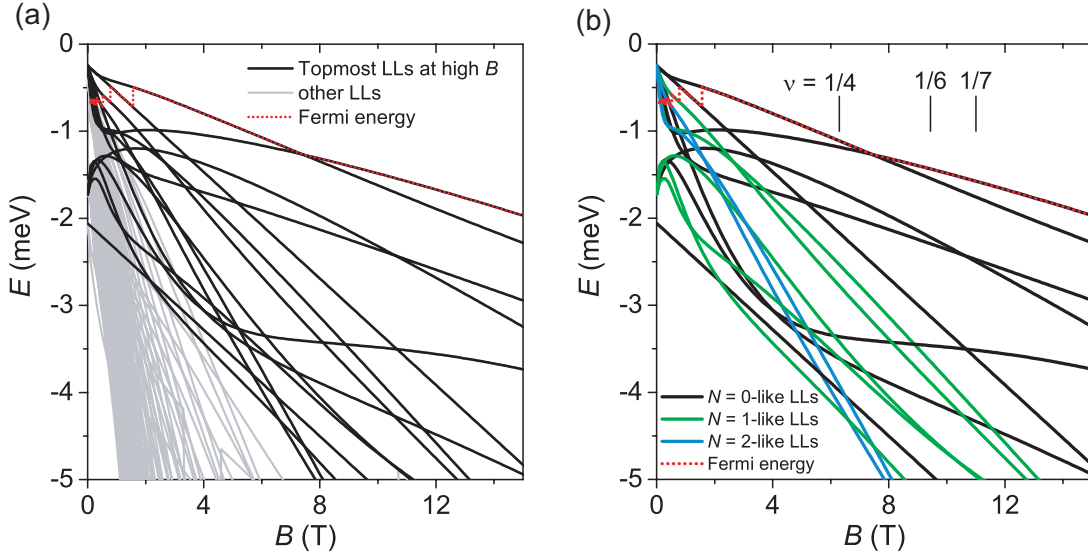


FIG. 12. **Landau level diagrams.** (a) Calculated E vs B Landau level diagram. The red dotted line traces the Fermi energy E_F . (b) Topmost LLs at high B are color-coded according to their dominant orbital component in the field range $4 < B < 12$ T where competing FQHSs and WC states are observed. B positions of typical fillings are marked with vertical lines.

spinors, written as:

$$\psi_{\mathcal{N}} = \sum_s |N = \mathcal{N} - s - \frac{3}{2}\rangle \xi_s^{\mathcal{N}} u_s \quad (\text{E1})$$

with $N \geq 0$. Here u_s are the base spinors with spin s and $\xi_s^{\mathcal{N}}$ give the relative weights of the HH and LH

spinors. $\mathcal{N} = 0, 1, 2, \dots$ are quantum numbers that label the energies of the LLs [33]. In Eq. (E1), a LL described by a particular quantum number \mathcal{N} can be decomposed into a basis of four spinors u_s , each of which can be described by a spin quantum number $s = \pm 1/2$ or $\pm 3/2$ and is coupled to a Landau harmonic oscillator with orbital quantum number $N = \mathcal{N} - s - \frac{3}{2}$. The relative

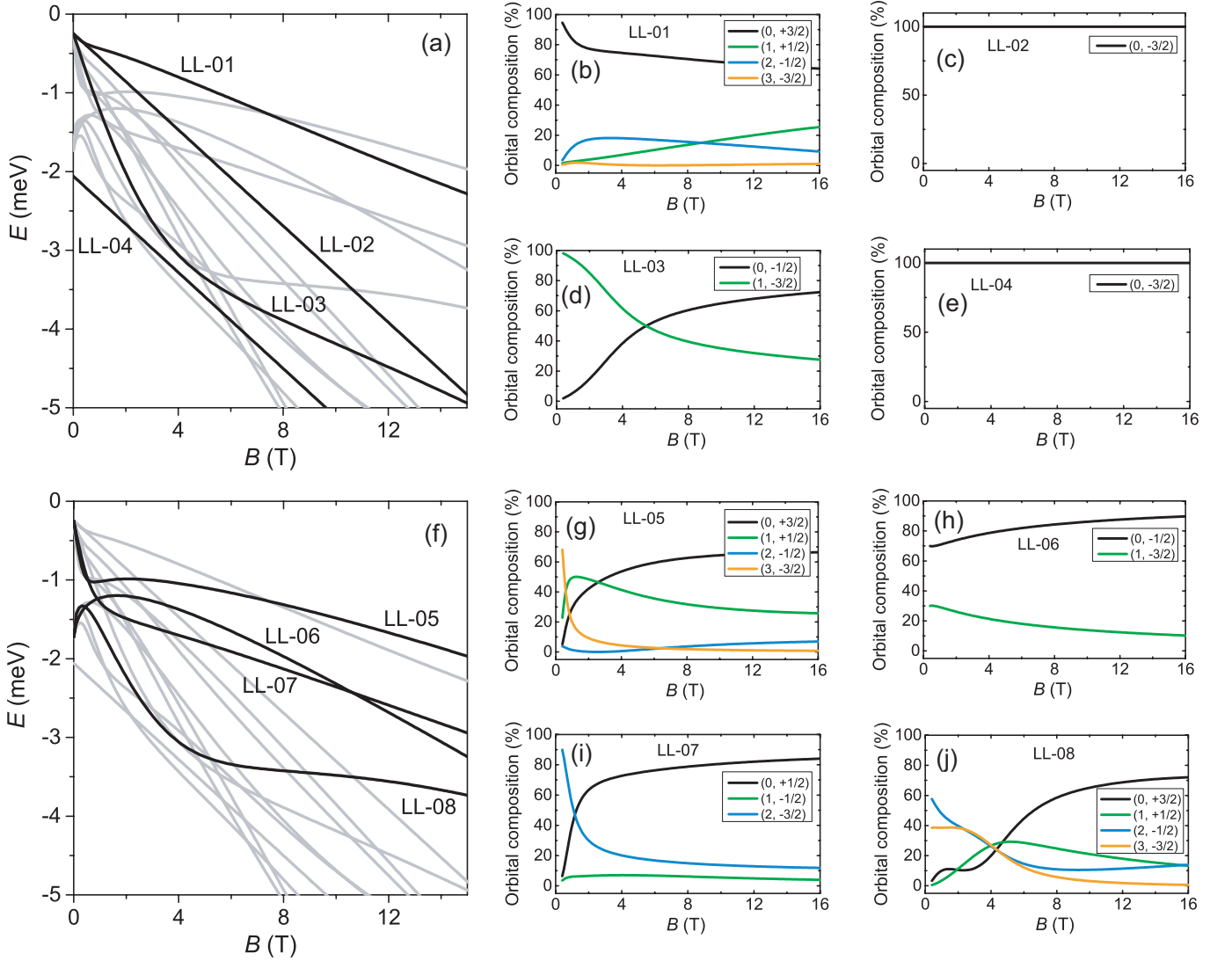


FIG. 13. $N = 0$ -like Landau levels and their orbital compositions. (a) E vs B LL diagram with LL-01, LL-02, LL-03, and LL-04 highlighted. (b-e) Orbital compositions for LL-01, LL-02, LL-03, and LL-04, respectively. The Landau orbital quantum number N and spin quantum number s_z are shown in the legend boxes as (N, s_z) . (f) E vs B LL diagram with LL-05, LL-06, LL-07, and LL-08 highlighted. (g-j) Orbital compositions for LL-05, LL-06, LL-07, and LL-08, respectively.

weight ξ_s^N of each spinor for a LL is equivalent to the relative weight of the $N = \mathcal{N} - s - \frac{3}{2}$ orbital component for this LL, providing information for LL orbital compositions. In Figs. 13-15, we present calculated orbital compositions for $N = 0$ -like, $N = 1$ -like, and $N = 2$ -like LLs shown in Fig. 12(b), respectively.

Some LLs are rather simple in their orbital compositions. For example, LL-02 is a purely $N = 0$, $s_z = -3/2$ LL [100% $(0, -3/2)$ component; see Fig. 13(c)] [58]. It has a linear E vs B dependence [see Fig. 13(a)], reminiscent of LLs for GaAs 2DESs. LL-02 is decoupled from all other LLs, because it has a quantum number $\mathcal{N} = 0$ and the only combination of N and s_z that meets the condition $\mathcal{N} = N + s + \frac{3}{2}$ is $N = 0$ and $s_z = -3/2$, denoted as $(0, -3/2)$. Other LLs, however, are more complex and

have up to four orbital components whose weights vary with B , leading to a highly nonlinear E vs B dependence. For some LLs, the leading orbital component even switches at finite B as a result of LL anti-crossings. Taking LL-03 as an example, it has two orbital components $(0, -1/2)$ and $(1, -3/2)$. While the $(1, -3/2)$ component dominates at low B , its weight decreases monotonically from 100% to 25% when B increases from 0 to 20 T, and as a result, the $(0, -1/2)$ component becomes dominant at high B . A crossover from the $N = 1$ -dominant regime to the $N = 0$ -dominant regime for LL-03 occurs at $\simeq 5$ T, consistent with a significant change in slope at $\simeq 5$ T in Fig. 13(a). Considering that we are interested in the physics at high B (≥ 5 T), LL-03 is categorized as a $N = 0$ -like LL. Similar logic is applied to categorize the

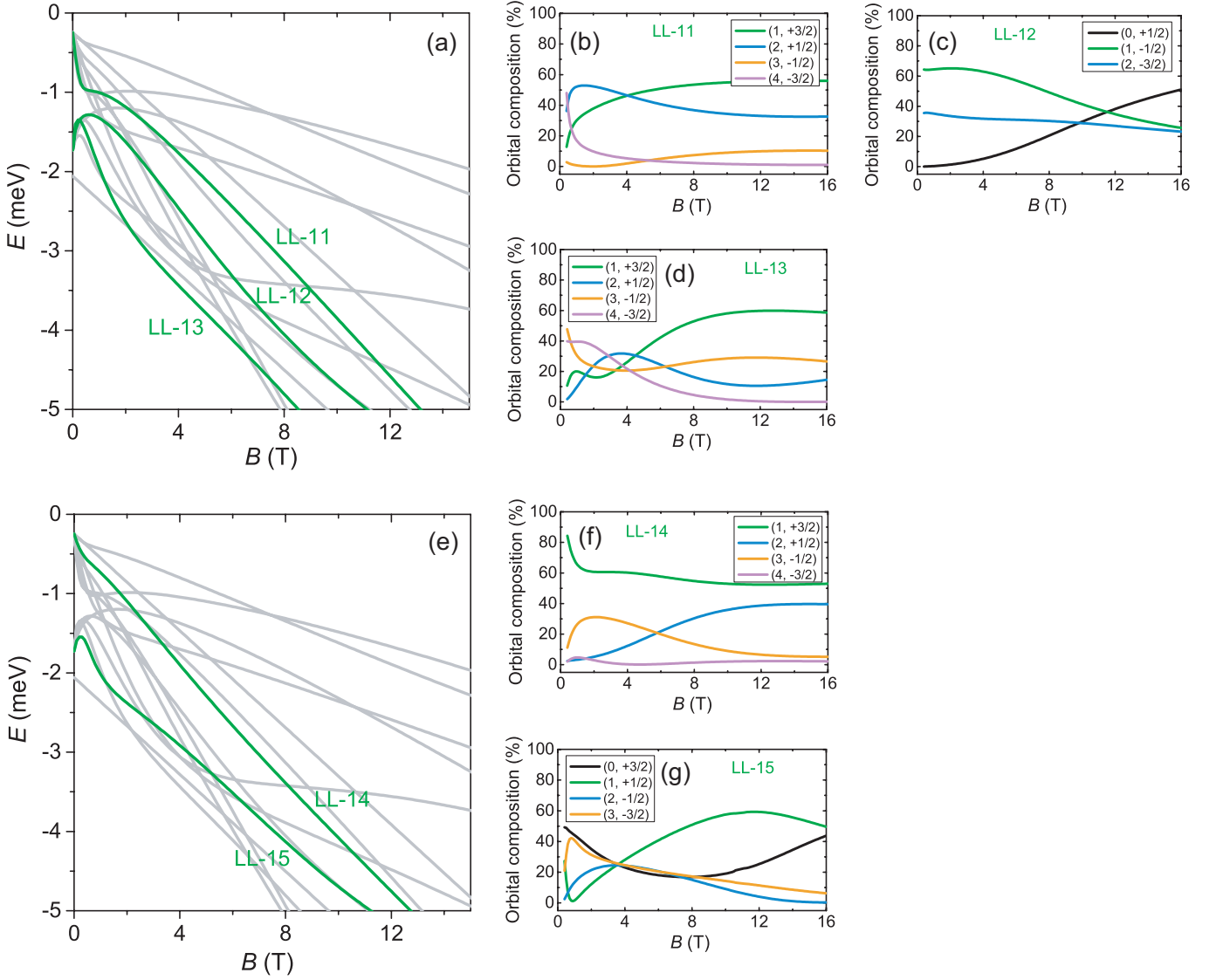


FIG. 14. $N = 1$ -like Landau levels and their orbital compositions. (a) E vs B LL diagram with LL-11, LL-12, and LL-13 highlighted. (b-d) Orbital compositions for LL-11, LL-12, and LL-13, respectively. (e) E vs B LL diagram with LL-14 and LL-15 highlighted. (f, g) Orbital compositions for LL-14 and LL-15, respectively.

LLs shown in Fig. 12(b).

As noted in Sec. IV.A, the ratio $E_{\text{Coul}}/\Delta E$ obtained from our calculated LL fan diagram provides a good estimate of the LLM parameter κ for our 2DHS. One may wonder whether this approach could offer insights into κ for various GaAs 2DHSs with different sample parameters. Our preliminary calculations suggest that at certain B , the ΔE values remain approximately consistent across GaAs 2DHSs with varying quantum well widths and densities. This consistency implies that the plot of $E_{\text{Coul}}/\Delta E$ vs B shown in Fig. 5(c) may serve as a reasonable estimate of κ for GaAs 2DHSs with diverse sample parameters.

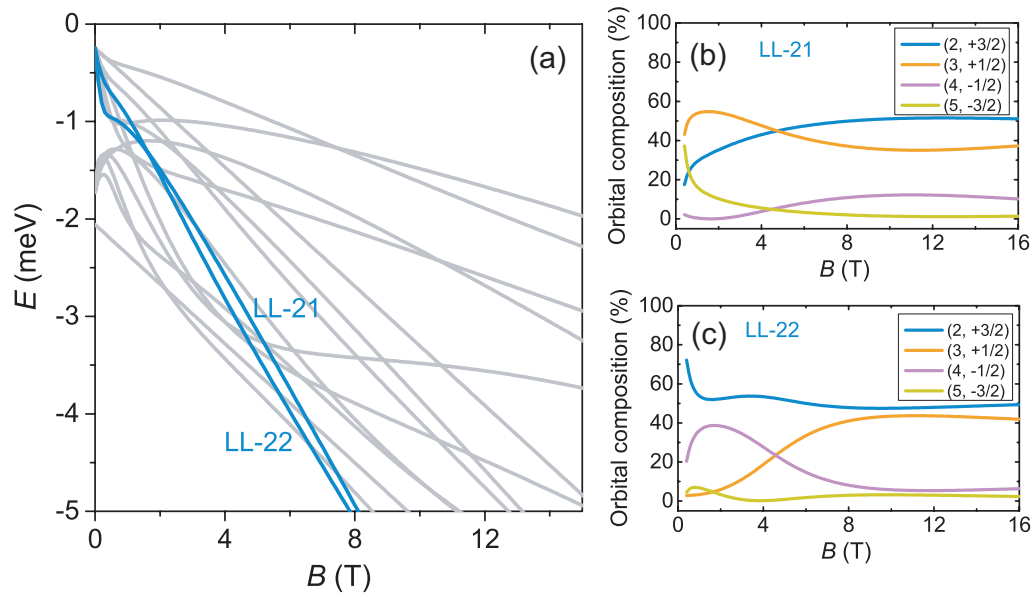


FIG. 15. $N = 2$ -like Landau levels and their orbital components. (a) E vs B LL diagram with LL-21 and LL-22 highlighted. (b, c) Orbital compositions for LL-21 and LL-22, respectively.

-
- [1] D. C. Tsui, H. L. Stormer, and A. C. Gossard, Two-Dimensional Magnetotransport in the Extreme Quantum Limit, *Phys. Rev. Lett.* **48**, 1559 (1982).
- [2] M. Shayegan, Flatland Electrons in High Magnetic Fields, in *High Magnetic Fields: Science and Technology*, edited by F. Herlach and N. Miura (World Scientific, Singapore, 2006), Vol. 3, pp. 31–60; arXiv:cond-mat/0505520.
- [3] J. K. Jain, *Composite Fermions*, (Cambridge University Press, Cambridge, England, 2007).
- [4] *Fractional Quantum Hall Effects: New Developments*, edited by B. I. Halperin and J. K. Jain (World Scientific, Singapore, 2020).
- [5] E. Wigner, On the Interaction of Electrons in Metals, *Phys. Rev.* **46**, 1002 (1934).
- [6] M. Shayegan, Wigner crystals in flat band 2D electron systems, *Nat. Rev. Phys.* **4**, 212 (2022).
- [7] E. Y. Andrei, G. Deville, D. C. Glattli, F. I. B. Williams, E. Paris, and B. Etienne, Observation of a Magnetically Induced Wigner Solid, *Phys. Rev. Lett.* **60**, 2765 (1988).
- [8] H. W. Jiang, R. L. Willett, H. L. Stormer, D. C. Tsui, L. N. Pfeiffer, and K. W. West, Quantum liquid versus electron solid around $\nu = 1/5$ Landau-level filling, *Phys. Rev. Lett.* **65**, 633 (1990).
- [9] V. J. Goldman, M Santos, M Shayegan, and J. E. Cunningham, Evidence for two-dimensional quantum Wigner crystal, *Phys. Rev. Lett.* **65**, 2189 (1990).
- [10] Y. P. Chen, G. Sambandamurthy, Z. H. Wang, R. M. Lewis, L. W. Engel, D. C. Tsui, P. D. Ye, L. N. Pfeiffer, and K. W. West, Melting of a 2D quantum electron solid in high magnetic field, *Nat. Phys.* **2**, 452 (2006).
- [11] H. Deng, Y. Liu, I. Jo, L. N. Pfeiffer, K. W. West, K. W. Baldwin, and M. Shayegan, Commensurability Oscillations of Composite Fermions Induced by the Periodic Potential of a Wigner Crystal, *Phys. Rev. Lett.* **117**, 096601 (2019).
- [12] H. Deng, L. N. Pfeiffer, K. W. West, K. W. Baldwin, L. W. Engel, and M. Shayegan, Probing the Melting of a Two-Dimensional Quantum Wigner Crystal via its Screening Efficiency, *Phys. Rev. Lett.* **122**, 116601 (2019).
- [13] M. B. Santos, Y. W. Suen, M. Shayegan, Y. P. Li, L. W. Engel, and D. C. Tsui, Observation of a Reentrant Insulating Phase Near the $1/3$ Fractional Quantum Hall Liquid in a Two-Dimensional Hole System, *Phys. Rev. Lett.* **68**, 1188 (1992).
- [14] M. B. Santos, J. Jo, Y. W. Suen, L. W. Engel, and M. Shayegan, Effect of Landau-level mixing on quantum-liquid and solid states of two-dimensional hole systems, *Phys. Rev. B* **46**, 13639(R) (1992).
- [15] Meng K. Ma, K. A. Villegas Rosales, H. Deng, Y. J. Chung, L. N. Pfeiffer, K. W. West, K. W. Baldwin, R. Winkler, and M. Shayegan, Thermal and Quantum Melting Phase Diagrams for a Magnetic-Field-Induced Wigner Solid, *Phys. Rev. Lett.* **125**, 036601 (2020).
- [16] K. A. Villegas Rosales, S. K. Singh, Meng K. Ma, Md. Shafayat Hossain, Y. J. Chung, L. N. Pfeiffer, K. W. West, K. W. Baldwin, and M. Shayegan, Competition between fractional quantum Hall liquid and Wigner solid at small fillings: Role of layer thickness and Landau level mixing, *Phys. Rev. Research* **3**, 013181 (2021).
- [17] S. K. Singh, A. Gupta, P. T. Madathil, C. Wang, K. W. Baldwin, L. N. Pfeiffer, and M. Shayegan, Developing fractional quantum Hall states at $\nu = 1/7$ and $\nu = 2/11$ in the presence of significant Landau-level mixing, *Phys. Rev. B* **110**, 165143 (2024).
- [18] D. Maryenko, A. McCollam, J. Falson, Y. Kozuka, J. Bruin, U. Zeitler, and M. Kawasaki, Composite fermion liquid to Wigner solid transition in the lowest Landau level of zinc oxide, *Nat. Comm.* **9**, 4356 (2018).
- [19] Yen-Chen Tsui, Minhao He, Yuwen Hu, Ethan Lake, Taige Wang, Kenji Watanabe, Takashi Taniguchi, Michael P Zaletel, and Ali Yazdani, Direct observation of a magnetic-field-induced Wigner crystal, *Nature* **628**, 287 (2024).
- [20] J. Nakamura, S. Liang, G. C. Gardner, and M. J. Manfra, Direct observation of anyonic braiding statistics, *Nat. Phys.* **16**, 931 (2020).
- [21] H. Bartolomei, M. Kumar, R. Bisognin, A. Marguerite, J.-M. Berroir, E. Bocquillon, B. Plaçaïs, A. Cavanna, Q. Dong, U. Gennser, Y. Jin, and G. Fève, Fractional statistics in anyon collisions, *Science* **368**, 173 (2020).
- [22] D. E. Feldman and B. I. Halperin, Fractional charge and fractional statistics in the quantum Hall effects, *Rep. Prog. Phys.* **84**, 076501 (2021).
- [23] Chetan Nayak, Steven H. Simon, Ady Stern, Michael Freedman, and Sankar Das Sarma, Non-Abelian anyons and topological quantum computation, *Rev. Mod. Phys.* **80**, 1083 (2008).
- [24] Mitali Banerjee, Moty Heiblum, Vladimir Umansky, Dima E. Feldman, Yuval Oreg, and Ady Stern, Observation of half-integer thermal Hall conductance, *Nature* **559**, 205 (2018).
- [25] R. L. Willett, K. Shtengel, C. Nayak, L. N. Pfeiffer, Y. J. Chung, M. L. Peabody, K. W. Baldwin, and K. W. West, Interference Measurements of Non-Abelian $e/4$ & Abelian $e/2$ Quasiparticle Braiding, *Phys. Rev. X* **13**, 011028 (2023).
- [26] V. J. Goldman, M. Shayegan, and D. C. Tsui, Evidence for the Fractional Quantum Hall State at $\nu = 1/7$, *Phys. Rev. Lett.* **61**, 881 (1988).
- [27] W. Pan, H. L. Stormer, D. C. Tsui, L. N. Pfeiffer, K. W. Baldwin, K. W. West, Transition from an electron solid to the sequence of fractional quantum Hall states at very low Landau level filling factor, *Phys. Rev. Lett.* **88**, 176802 (2002).
- [28] Yoon Jang Chung, D. Graf, L. W. Engel, K. A. Villegas Rosales, P. T. Madathil, K. W. Baldwin, K. W. West, L. N. Pfeiffer, and M. Shayegan, Correlated States of 2D Electrons near the Landau Level Filling $\nu = 1/7$, *Phys. Rev. Lett.* **128**, 026802 (2022).
- [29] Chengyu Wang, P. T. Madathil, S. K. Singh, A. Gupta, Y. J. Chung, L. N. Pfeiffer, K. W. Baldwin, and M. Shayegan, Developing fractional quantum Hall states at even-denominator fillings $1/6$ and $1/8$, *Phys. Rev. Lett.* **134**, 046502 (2025).
- [30] H. Zhu, K. Lai, D. C. Tsui, S. P. Bayrakci, N. P. Ong, M. Manfra, L. Pfeiffer, and K. West, Density and well width dependences of the effective mass of two-dimensional holes in (100) GaAs quantum wells measured using cyclotron resonance at microwave frequencies, *Solid State Commun.* **141**, 510 (2007).

- [31] Yang Liu, S. Hasdemir, A. Wójs, J. K. Jain, L. N. Pfeiffer, K. W. West, K. W. Baldwin, and M. Shayegan, Spin polarization of composite fermions and particle-hole symmetry breaking, *Phys. Rev. B* **90**, 085301 (2014).
- [32] In the context of GaAs 2DHSs, the word "mixing" is also commonly used to describe the coupling between heavy holes and light holes, known as heavy-hole light-hole mixing [33]. To distinguish it from the LLM we discuss throughout this article, we use the phrase heavy-hole light-hole *coupling* instead. In Appendix E, we elaborate on the complex nature of hole LLs as a consequence of heavy-hole light-hole coupling.
- [33] R. Winkler, *Spin-Orbit Coupling Effects in Two-Dimensional Electron and Hole Systems*, (Springer, Berlin, 2003).
- [34] Michael R. Peterson and Chetan Nayak, Effects of Landau Level Mixing on the Fractional Quantum Hall Effect in Monolayer Graphene, *Phys. Rev. Lett.* **113**, 086401 (2014).
- [35] Edward H. Rezayi, Landau Level Mixing and the Ground State of the $\nu = 5/2$ Quantum Hall Effect, *Phys. Rev. Lett.* **119**, 026801 (2017).
- [36] Jianyun Zhao, Yuhe Zhang, and J. K. Jain, Crystallization in the Fractional Quantum Hall Regime Induced by Landau-Level Mixing, *Phys. Rev. Lett.* **121**, 116802 (2018).
- [37] Md. S. Hossain, T. Zhao, S. Pu, M. A. Mueed, M. K. Ma, K. A. V. Rosales, Y. J. Chung, L. N. Pfeiffer, K. W. West, K. W. Baldwin, J. K. Jain, and M. Shayegan, Bloch ferromagnetism of composite fermions, *Nat. Phys.* **17**, 48 (2021).
- [38] Chengyu Wang, A. Gupta, S. K. Singh, Y. J. Chung, L. N. Pfeiffer, K. W. West, K. W. Baldwin, R. Winkler, and M. Shayegan, Even-Denominator Fractional Quantum Hall State at Filling Factor $\nu = 3/4$, *Phys. Rev. Lett.* **129**, 156801 (2022).
- [39] Chengyu Wang, Adbhut Gupta, Pranav T. Madathil, Siddharth K. Singh, Yoon Jang Chung, Loren N. Pfeiffer, Kirk W. Baldwin, and Mansour Shayegan, Next-generation even-denominator fractional quantum Hall states of interacting composite fermions, *Proc. Natl. Acad. Sci. U.S.A.* **120**, e2314212120 (2023).
- [40] Chengyu Wang, A. Gupta, S. K. Singh, P. T. Madathil, Y. J. Chung, L. N. Pfeiffer, K. W. Baldwin, R. Winkler, and M. Shayegan, Fractional Quantum Hall State at Filling Factor $\nu = 1/4$ in Ultra-High-Quality GaAs Two-Dimensional Hole Systems, *Phys. Rev. Lett.* **131**, 266502 (2023).
- [41] Tongzhou Zhao, Ajit C. Balram, and J. K. Jain, Composite fermion pairing induced by Landau level mixing, *Phys. Rev. Lett.* **130**, 186302 (2023).
- [42] Sudipto Das, Sahana Das, and Sudhansu S. Mandal, Anomalous Reentrant $5/2$ Quantum Hall Phase at Moderate Landau-Level-Mixing Strength, *Phys. Rev. Lett.* **131**, 056202 (2023).
- [43] Yoon Jang Chung, C. Wang, S. K. Singh, A. Gupta, K. W. Baldwin, K. W. West, R. Winkler, M. Shayegan, and L. N. Pfeiffer, Record-quality GaAs two-dimensional hole systems, *Phy. Rev. Mater.* **6**, 034005 (2022).
- [44] Adbhut Gupta, C. Wang, S. K. Singh, K. W. Baldwin, R. Winkler, M. Shayegan, and L. N. Pfeiffer, Ultraclean two-dimensional hole systems with mobilities exceeding 10^7 cm²/Vs, *Phys. Rev. Mater.* **8**, 014004 (2024).
- [45] Yoon Jang Chung, K. A. Villegas Rosales, K. W. Baldwin, P. T. Madathil, K. W. West, M. Shayegan and L. N. Pfeiffer, Ultra-high-quality two-dimensional electron systems, *Nat. Mater.* **20**, 632-637 (2021).
- [46] R. L. Willett, R. R. Ruel, K. W. West, and L. N. Pfeiffer, Experimental demonstration of a Fermi surface at one-half filling of the lowest Landau level, *Phys. Rev. Lett.* **71**, 3846 (1993).
- [47] Alexander C. Archer, Kwon Park, and Jainendra K. Jain, Competing Crystal Phases in the Lowest Landau Level, *Phys. Rev. Lett.* **111**, 146804 (2013).
- [48] Alexander C. Archer and Jainendra K. Jain, Quantum bubble defects in the lowest-Landau-level crystal, *Phys. Rev. B* **90**, 201309 (2014).
- [49] P. T. Madathil, C. Wang, S. K. Singh, A. Gupta, K. A. Villegas Rosales, Y. J. Chung, K. W. West, K. W. Baldwin, L. N. Pfeiffer, L. W. Engel, and M. Shayegan, Signatures of Correlated Defects in an Ultraclean Wigner Crystal in the Extreme Quantum Limit, *Phys. Rev. Lett.* **132**, 096502 (2024).
- [50] P. T. Madathil, K. A. Villegas Rosales, Y. J. Chung, K. W. West, K. W. Baldwin, L. N. Pfeiffer, L. W. Engel, and M. Shayegan, Moving Crystal Phases of a Quantum Wigner Solid in an Ultra-High-Quality 2D Electron System, *Phys. Rev. Lett.* **131**, 236501 (2023).
- [51] R. L. Willett, H. L. Stormer, D. C. Tsui, L. N. Pfeiffer, K. W. West, and K. W. Baldwin, Termination of the series of fractional quantum hall states at small filling factors, *Phys. Rev. B* **38**, 7881(R) (1988).
- [52] H. W. Jiang, H. L. Stormer, D. C. Tsui, L. N. Pfeiffer, and K. W. West, Magnetotransport studies of the insulating phase around $\nu = 1/5$ Landau-level filling, *Phys. Rev. B* **44**, 8107 (1991).
- [53] Yang Liu, S. Hasdemir, D. Kamburov, A. L. Graninger, M. Shayegan, L. N. Pfeiffer, K. W. West, K. W. Baldwin, and R. Winkler, Even-denominator fractional quantum Hall effect at a Landau level crossing, *Phys. Rev. B* **89**, 165313 (2014).
- [54] Yang Liu, M. A. Mueed, Md. Shafayat Hossain, S. Hasdemir, L. N. Pfeiffer, K. W. West, K. W. Baldwin, and M. Shayegan, Morphing of two-dimensional hole systems at $\nu = 3/2$ in parallel magnetic fields: Compressible, stripe, and fractional quantum Hall phases, *Phys. Rev. B* **94**, 155312 (2016).
- [55] M. Lupatini, P. Knüppel, S. Faelt, R. Winkler, M. Shayegan, A. Imamoglu, and W. Wegscheider, Spin Reversal of a Quantum Hall Ferromagnet at a Landau Level Crossing, *Phys. Rev. Lett.* **125**, 067404 (2020).
- [56] Meng K. Ma, Chengyu Wang, Y. J. Chung, L. N. Pfeiffer, K. W. West, K. W. Baldwin, R. Winkler, and M. Shayegan, Robust Quantum Hall Ferromagnetism near a Gate-Tuned $\nu = 1$ Landau Level Crossing, *Phys. Rev. Lett.* **129**, 196801 (2022).
- [57] Chengyu Wang, A. Gupta, Y. J. Chung, L. N. Pfeiffer, K. W. West, K. W. Baldwin, R. Winkler, M. Shayegan, Highly-Anisotropic Even-Denominator Fractional Quantum Hall State in an Orbitally-Coupled Half-Filled Landau Level, *Phys. Rev. Lett.* **131**, 056302 (2023).
- [58] D. A. Broido and L. J. Sham, Effective masses of holes at GaAs-AlGaAs heterojunctions, *Phys. Rev. B* **31**, 888 (1985).
- [59] In GaAs 2DESs, where LLs are strictly linear with B , ΔE is simply equal to E_{cyc} . It is noteworthy that, for our 2DHS, between the topmost $N = 0$ -like and $N = 1$ -like LLs, there are multiple other $N = 0$ -like LLs whose

leading spinor components have different spin quantum numbers $s_z = \pm 3/2$ and $\pm 1/2$. Some of these LLs originate from the second electric subband of the QW; see Appendix E for details of the spinor composition of these LLs. Here we ignore these LLs in our definition of ΔE because the separations between the lowest LL and these other $N = 0$ LLs, in principle, do not affect the cyclotron energy. The effect of multiple $N = 0$ LLs near the lowest LL is not negligible, and is not captured by κ . The role of the proximity of these $N = 0$ LLs to the lowest LL is also important, but beyond the scope of this article.

- [60] Note that both $E_{\text{Coul}}/E_{\text{cyc}}$ and $E_{\text{Coul}}/\Delta E$ here provide only rough estimations of κ . This is because hole LLs are not evenly spaced in E as a consequence of their nonlinearity, and each hole LL is a superposition of four spinors with different N , as described in the text and Appendix E.
- [61] Yoon Jang Chung, A. Gupta, K. W. Baldwin, K. W. West, M. Shayegan, and L. N. Pfeiffer, Understanding limits to mobility in ultrahigh-mobility GaAs two-dimensional electron systems: 100 million cm^2/Vs and beyond, *Phys. Rev. B* **106**, 075134 (2022).
- [62] J. K. Jain, private communication.
- [63] Yoon Jang Chung, K. A. Villegas Rosales, H. Deng, K. W. Baldwin, K. W. West, M. Shayegan, and L. N. Pfeiffer, Multivalley two-dimensional electron system in an AlAs quantum well with mobility exceeding $2 \times 10^6 \text{ cm}^2 \text{ V}^{-1} \text{ s}^{-1}$, *Phys. Rev. Mater.* **2**, 071001(R) (2018).
- [64] Zheng-Wei Zuo, Ajit C. Balram, Songyang Pu, Jianyun Zhao, Thierry Jolicoeur, A. Wójs, and J. K. Jain, Interplay between fractional quantum Hall liquid and crystal phases at low filling, *Phys. Rev. B* **102**, 075307 (2020).
- [65] V. J. Goldman, J. K. Wang, B. Su, and M. Shayegan, Universality of the Hall effect in a magnetic-field-localized two-dimensional electron system, *Phys. Rev. Lett.* **70**, 647 (1993).
- [66] T. Sajoto, Y. P. Li, L. W. Engel, D. C. Tsui, and M. Shayegan, Hall resistance of the reentrant insulating phase around the $1/5$ fractional quantum Hall liquid, *Phys. Rev. Lett.* **70**, 2321 (1993).
- [67] Y. W. Suen, L. W. Engel, M. B. Santos, M. Shayegan, and D. C. Tsui, Observation of a $\nu = 1/2$ fractional quantum Hall state in a double-layer electron system, *Phys. Rev. Lett.* **68**, 1379 (1992).
- [68] S. K. Singh, C. Wang, C. T. Tai, C. S. Calhoun, K. A. Villegas Rosales, P. T. Madathil, A. Gupta, K. W. Baldwin, L. N. Pfeiffer, M. Shayegan, Topological phase transition between Jain states and daughter states of the $\nu = 1/2$ fractional quantum Hall state, *Nat. Phys.* **20**, 1247 (2024).